Electronic Supplementary Information (ESI) for

Non-nucleophilic electrolyte with non-fluorinated hybrid solvents for long-life magnesium metal batteries

Yue Sun,[a] Yuhang Wang,[b] Liwei Jiang,[a] Dejian Dong,[a] Wanwan Wang,[a] Jun Fan [b] and Yi-Chun Lu *[a]

[a] Electrochemical Energy and Interfaces Laboratory, Department of Mechanical and Automation Engineering, The Chinese University of Hong Kong, Shatin, N.T., 999077 Hong Kong, SAR, China.

[b] Department of Materials Science and Engineering, City University of Hong Kong, Kowloon 999077, Hong Kong, SAR, China.

Corresponding Author

*E-mail: yichunlu@mae.cuhk.edu.hk

Experimental methods

Materials. Magnesium bis(trifluoromethanesulfonyl)imide ($Mg(TFSI)_2$, 97%, TCI) was dried in a glass oven (Büchi) at 240 °C for 24 h under vacuum and transferred to Ar-filled glove box (Etelux, H_2O < 1.0 ppm, O_2 < 1.0 ppm). Magnesium chloride ($MgCl_2$, anhydrous, ≥98%), poly(tetrafluoroethylene) (PTFE, 60% suspension in water) and 2-propanol (anhydrous, 99.5%) were received from Sigma-Aldrich. Molybdenum sulfide (MoS_2, 99.5%) and iodine (I_2, 99.8%) were received from Macklin. Copper powders (Cu, 99.9%) were received from Meryer and molybdenum powders (Mo, 99.95%) were received from Alfa Aesar. 1,2-dimethoxyethane (DME, anhydrous, 99.5%, Sigma-Aldrich) and 1,3-dioxane (DOL, anhydrous, 99.8%, Sigma-Aldrich) were dried with activated 4Å molecular sieves (Sigma-Aldrich). Tetrahydrofuran (THF, anhydrous, 99.9%, Sigma-Aldrich) and 2-methyltetrahydrofuran (2-MeTHF, anhydrous, 99%, Meryer) were dried with 3Å molecular sieves (Meryer) for one week to remove moisture.

Cathode fabrication. Mo_6S_8 was synthesized according to previous report.[1] The MoS_2, Cu, Mo, and iodine powders were milled under Ar, and the mixture was heated to 800 ℃ at 2 ℃ min^{-1} and kept under Ar for 24 hours.[1] Then Cu in obtained $Cu_2Mo_6S_8$ precursors was leached out in 6 M HCl solution for 12 h with O_2 bubbling.[1] Mo_6S_8 was mixed with Ketjen Black EC-600JD (KB, AzkoNobel) and PTFE in IPA at the weight ratio of 8:1:1, then the electrode was prepared via compressing the mixture on a Φ12 mm × 0.1 mm Mo mesh.

Electrolyte preparation. 0.8 M $Mg(TFSI)_2$-$2MgCl_2$ (MTC) was prepared by adding 584 mg $Mg(TFSI)_2$ and 190 mg $MgCl_2$ in 1 ml DME and stirring at 70 °C for half an hour. Then the solutions with 0.2 M MTC and 0 ~ 75 vol % THF were obtained via diluting the saturated 0.8 M solutions with 3 ml DME / THF / binary mixtures.

Electrochemistry. All the two-electrode cells were assembled with a piece of Φ12 mm × 0.1 mm Mg disc (polished under Ar gas), a piece of quartz fiber (Φ16 mm × 1.0 mm, Whatman) and Mo_6S_8 cathode. Quartz fibers were dried in glass oven under vacuum at 150 ^oC overnight to remove the moisture. All the cells were assembled in glove box under Ar gas and tested in 2032-type coin-cell configuration. All the electrochemical test was carried out with LAND Battery Testing System (Land, Wuhan Land Electronic Co., Ltd.) and VMP3 electrochemical testing unit (Bio-Logic, France) at 25 ℃. All the electrochemical performance data was obtained based on three-times measurement. Coulombic efficiency was measured with Mg-Cu cells under 1.0 mA cm^{-2}, 1.0 mAh cm^{-2} according to previous report.[2] 10 mAh cm^{-2} Mg^0 was deposited on the Cu cathode by discharging the Mg-Cu cells for 10 hours, then 1.0 mAh cm^{-2} Mg^0 was cycled between Cu cathode and Mg anode under 1.0 mA cm^{-2}. After 20 cycles, all the Mg^0 deposited on the Cu cathode was removed by charging the Mg-Cu cells to 1.0 V vs Mg/Mg^{2+}, and the corresponding charge capacity was recorded as Q_s. Therefore, the average CE is equal to $(20+Q_s)/30\times100$ %.

Materials characterizations. All the samples were washed with DME/THF for three times with Ar protection to remove the residue salts. SEM and EDS were performed on a field emission scanning electron microscopy (HR-FESEM) (FEI, Quanta 400). X-ray photoelectron spectroscopy (XPS) analysis was performed with Thermo Scientific K-Alpha+ (Thermo Fisher Scientific Inc.) using the mono Al Kα radiation (1486.6 eV) at the pressure lower than 5.0×10^{-9} mbar. The obtained XPS spectra were calibrated by C1s at 284.8 eV and fitted with CASA. *In-situ* FT-IR spectra were collected by Nicolet iS50 FTIR Spectrometer employing a two-electrode cell with diamond window. Atomic force microscopy (AFM) was performed using Nanoscope V Multimode 8 scanning probe microscope (Bruker). Nuclear magnetic resonance spectra were obtained with

Bruker AVANCE III 400 NMR Spectrometer in $CDCl_3$.

Computational details. All the calculations basing on density functional theory (DFT) were conducted by employing Vienna *ab initio* simulation package (VASP).[3,4] The projector augmented wave (PAW) method[5] was performed to describe the ion-electrons interactions. The exchange and correlation interaction was described by generalized gradient approximation (GGA) of Perdew-Burke-Ernzerhof (PBE) functional[6,7]. Dispersion correction method of DFT-D3 was used to correct the van der Waals (vdWs) interaction[8]. The convergence criteria for energy was set as 10^{-5} eV, the atomic positions were fully relaxed and the threshold for force was set to be 0.02 eV/Å. Subsequently, the cut-off energy of plane wave expansion was considered as 500 eV. A vacuum layer of 20 Å in *z* direction was adopted for the following calculation. The lowest energy surface for Mg and MgO was performed for calculations. And the geometry optimization was performed based on a *k*-point mech of 3 × 3 × 1.

For Mg, the conresponding surface was (0001), as confirm by previous literatures.[9,10] The 4 × 4 supercell containing 80 atoms and five surface layers with physical dimensions of 12.84 Å × 12.84 Å was used. The two bottom layers was fixed as their bulk spacing. According to the previous report[11], the (100) termination of MgO was adopted, with a 3 × 3 supercell (lattice parameter: a = b = 12.62 Å). The substrate included five layers and 90 Mg and 90 O atoms. The bottom two layers of atoms were fixed.

The adsorption energy, E_{ads}, for THF/DME on each surface was calculated as

$$E_{\mathrm{ads}} = E_{\mathrm{surf+THF/DME}} - E_{\mathrm{surf}} - E_{\mathrm{THF/DME}}$$

where $E_{\mathrm{surf+THF/DME}}$ is the total energy of the adsorbed THF/DME and surface system, E_{surf} is the total energy of the surface, and $E_{\mathrm{THF/DME}}$ is the energy of the isolated THF/DME molecule. Considering that adsorption energies calculated via DFT are

typically regarding to a gas-phase molecule, the liquid state reference is more physically realistic due to the adsorbate will be a liquid phase in a real battery. The energy of the liquid state for THF/DME was determined by subtracting the latent heat of vaporization ($\Delta_{vap}H$) from the gas phase energy. The $\Delta_{vap}H$ for THF and DME are 36 and 32 kJ/mol, respectively.[12] All the structures are visualized by VESTA software.[13]

Table S1. Summary of representative nucleophilic and non-nucleophilic salts for RMBs.

Nucleophilic electrolytes		Grignard reagents such as amidomagnesium halides and alkylmagnesium halides.[14]
		Dichloride complex (DCC): 2(Bu_2Mg) – $EtAlCl_2$.[15]
		"All phenyl" complex (APC): 2($PhMgCl_2$)–$AlCl_3$.[16]
Non-nucleophilic electrolytes	Chloride-based electrolytes	$Mg(TFSI)_2$/$Mg(Otf)_2$-$MgCl_2$.[17–20]
		$MgCl_2$-$AlCl_3$.[21–23]
	Weakly-coordinating-anion-based salts	Magnesium tetrakis(hexafluoroisopropyloxy)borate: $Mg[B(Ohfip)_4]_2$.[24,25]
		Magnesium closo-carbadodecaborate: $Mg(CB_{11}H_{12})_2$.[26,27]
		Magnesium perfluorinated tert-butoxide $Mg(pftb)_2$.[28]
		Magnesium perfluorinated pinacolatoaluminate (MgFPA). [28–30]

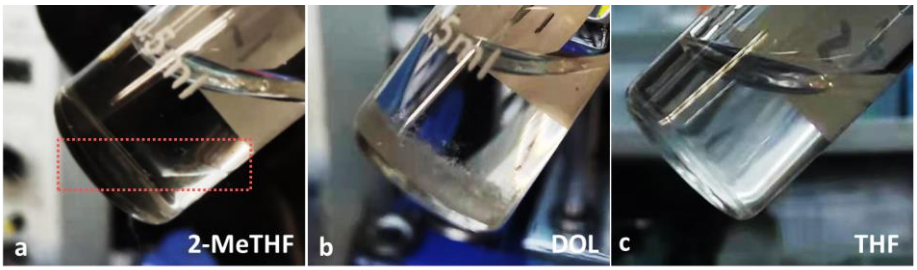

Fig. S1. Digital photographs of (a) DME-2MeTHF, (b) DME-DOL, (c) DME-THF (75 vol%) electrolytes.

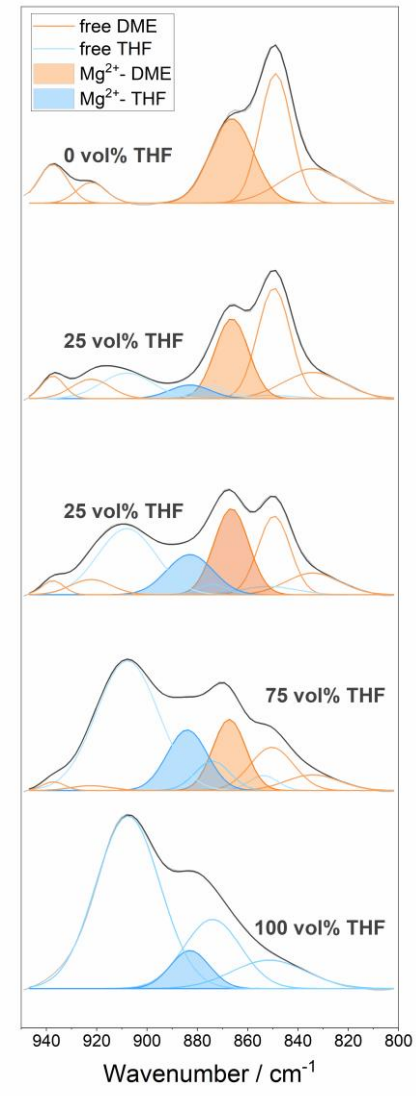

Fig. S2. Deconvoluted peaks in *ex-situ* FT-IR spectra of DME, DME-THF (25~75 vol% THF), and THF electrolytes.

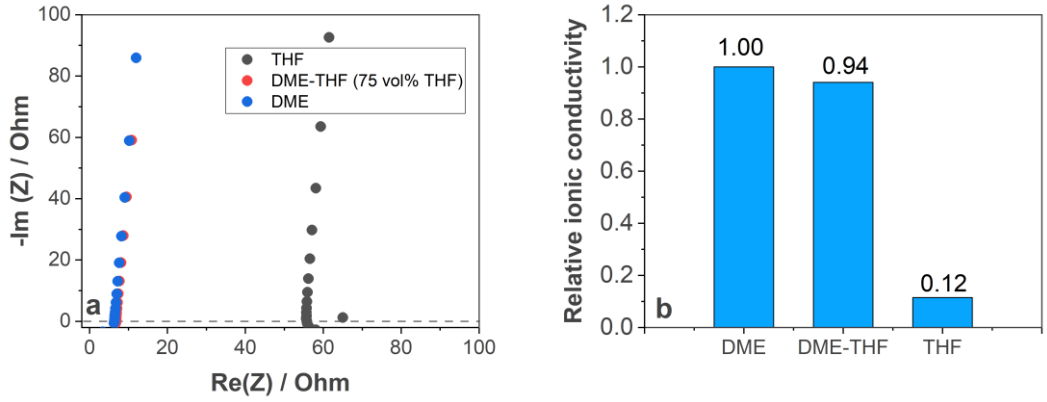

Fig. S3. (a) Nyquist plots of electrochemical impedance spectroscopy (EIS) over 1.2 kHz ~ 1.0 MHz for SS-SS symmetric cells with DME, DME-THF, and THF electrolytes. (b) Relative ionic conductivities compared with DME electrolytes. The first intercepts (R_x) with x-axis revealed the relative ionic conductivity with DME electrolytes according to the equation below[31]:

$$Relative\ ionic\ conductivity = \frac{R_{DME}}{R_x}$$

Although THF resulted in ten times lower ionic conductivity if serving as single solvent, similar ionic conductivity was retained if both DME and THF were involved.

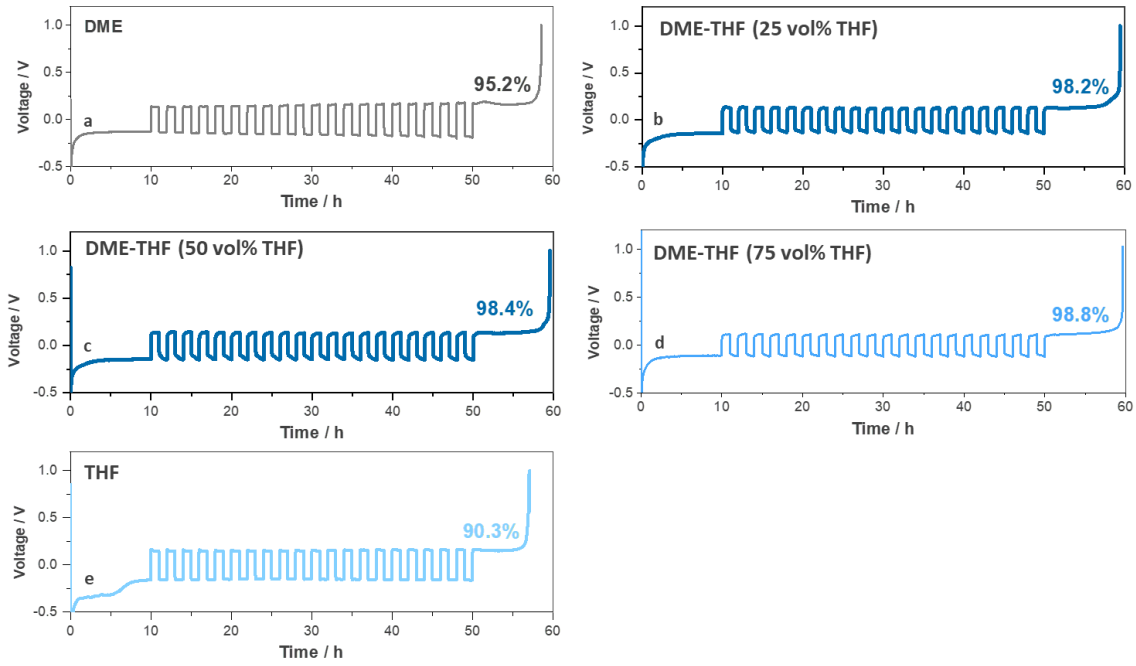

Fig. S4. Voltage profile of Mg-Cu cells with 0.2 M MTC in (a) pure DME, (b) DME-THF (25 vol% THF), (c) DME-THF (50 vol% THF), (d) DME-THF (75 vol% THF) and (e) pure THF.

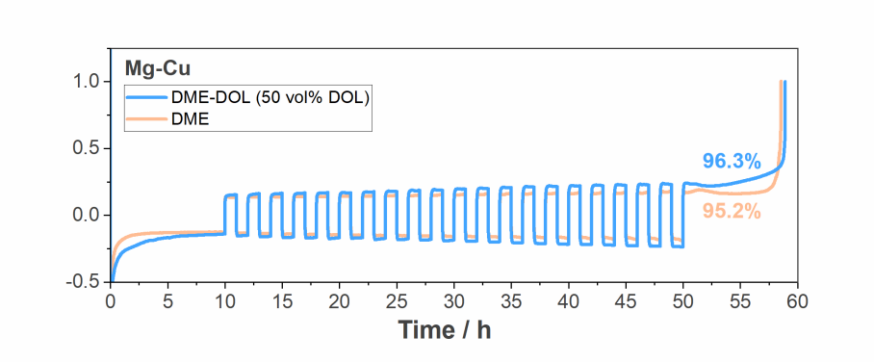

Fig. S5. Voltage profile of Mg-Cu cells with DME (yellow line) and DME-DOL (50 vol% DOL) electrolytes.

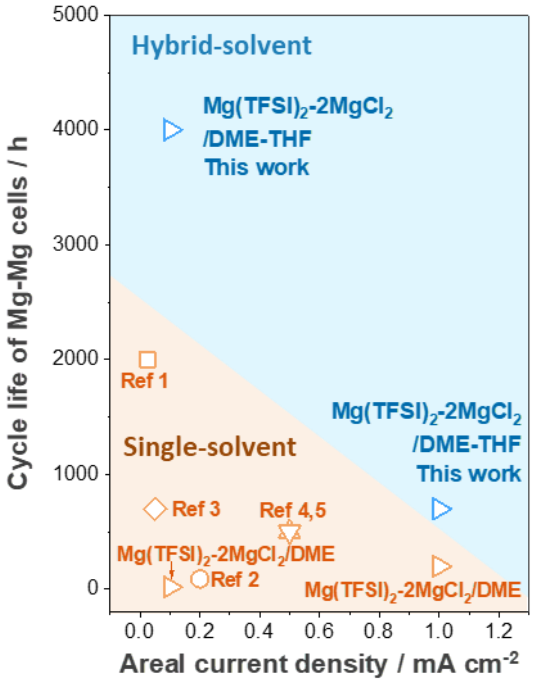

Fig. S6. Comparison of cycle life of Mg-Mg symmetric cells under different current densities with single-solvent and hybrid-solvent commercial $MgCl_2$-based electrolytes. Ref 1: $MgCl_2$-$AlCl_3$-$Mg(TFSI)_2$/DME[21]; Ref 2: $MgCl_2$-$AlCl_3$-$Mg(TFSI)_2$/THF[22]; Ref 3: $MgCl_2$-LiCl/THF[32]; Ref 4: $Mg(OTf)_2$-$MgCl_2$/DME[17]; Ref 5: $MgCl_2$-LiCl-$AlCl_3$-PYR14TFSI/THF[33].

Table S2. Summary of cycle life of Mg-Mg symmetric cells under different current densities with single-solvent and hybrid-solvent commercial $MgCl_2$-based electrolytes.

Electrolyte	Current density of Mg-Mg symmetric cells / mA cm^{-2}	Cycle life / hour	Reference
$Mg(TFSI)_2$-$MgCl_2$ / DME-THF	**0.1**	**4000**	**This work**
	1.0	**700**	
$MgCl_2$-$AlCl_3$-$Mg(TFSI)_2$ / DME	0.025	2000	[21]
$MgCl_2$-$AlCl_3$-$Mg(TFSI)_2$/THF	0.200	90	[22]
$MgCl_2$-LiCl / THF	0.05	700	[32]
$Mg(OTf)_2$-$MgCl_2$ / DME	0.500	500	[17]
$MgCl_2$-LiCl-$AlCl_3$-PYR14TFSI / THF	0.500	500	[33]

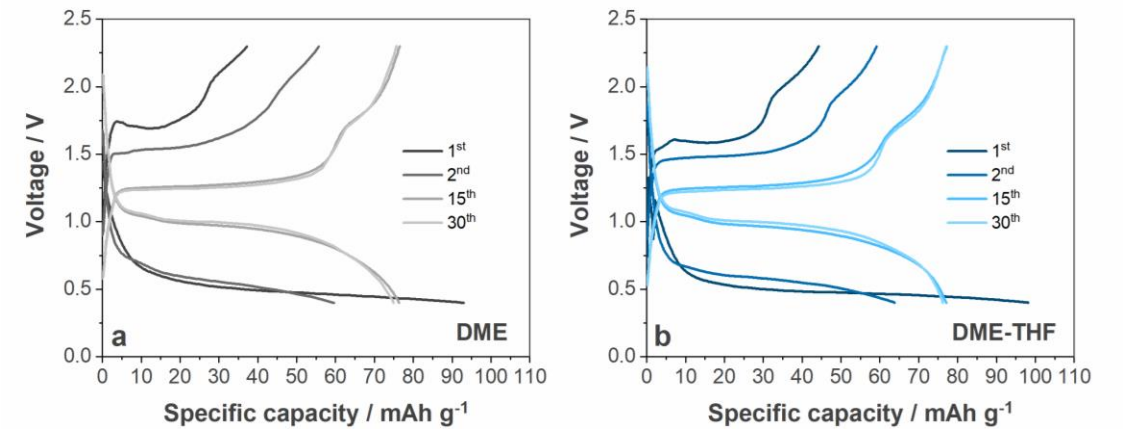

Fig. S7. Voltage profile of Mg-Mo_6S_8 cells during 1st~30th cycles under 0.5 C. (a) Cells with DME electrolytes. (b) Cells with DME-THF electrolytes.

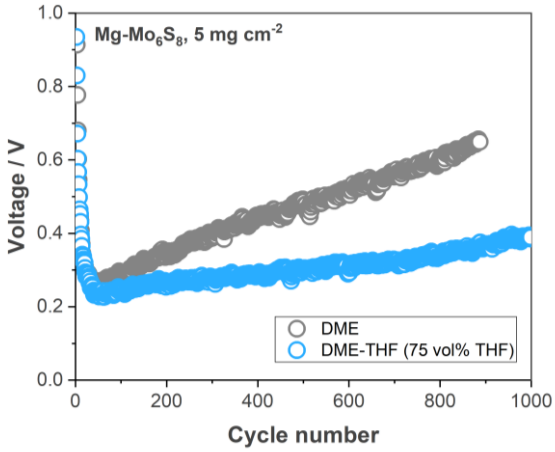

Fig. S8. Polarization of Mg-Mo_6S_8 cells with DME and DME-THF (75 vol% THF) electrolytes.

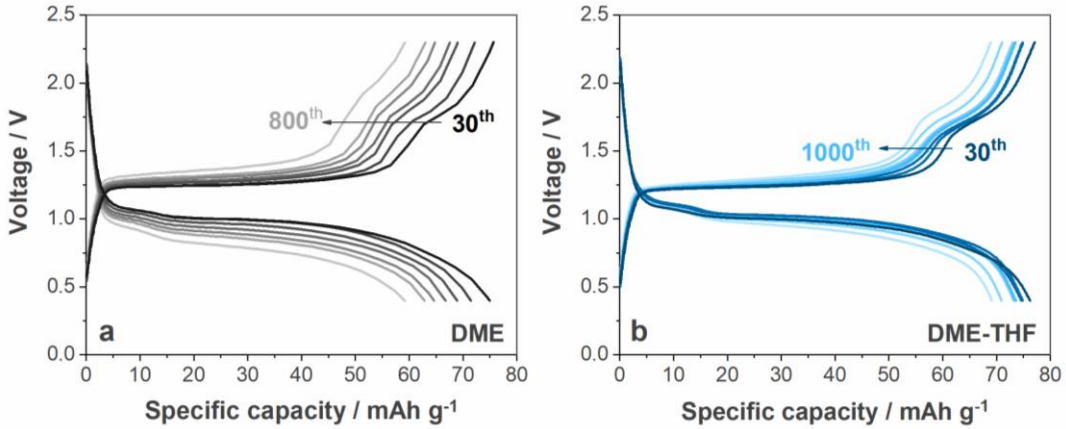

Fig. S9. Voltage profile of Mg-Mo_6S_8 cells after 30th cycle under 0.5 C. (a) Cells with DME electrolytes. (b) Cells with DME-THF electrolytes.

Table S3. Summary of the electrochemical performance of state-of-the-art Mg-Mo_6S_8 cells with electrolytes based on commercial salts.

Electrolyte		Rate / C	Cycle life / hour	Reference
Non-nucleophilic electrolytes	**$Mg(TFSI)_2$-$MgCl_2$ / DME-THF**	**0.5**	**2300**	**This work**
	$Mg(OTf)_2$-$MgCl_2$ / DME	0.1	1267	[17]
	$MgCl_2$-$AlCl_3$-$Mg(TFSI)_2$/THF	0.2	833	[22]
	$Mg(TFSI)_2$ / DME-diglyme	0.05	~200	[34]
	$Mg(HMDS)_2$-$4MgCl_2$ / THF	0.1	667	[35]
Nucleophilic electrolytes	$MgAlCl_2BuEt_2$ / THF	0.5	2286	[15]
	PhMgCl-$AlCl_3$ / THF	0.5	1500	[1]

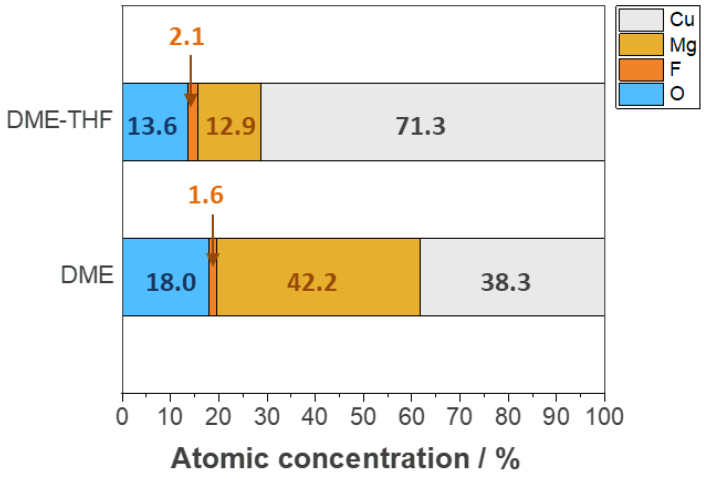

Fig. S10. The atomic concentration of Mg, F, O, and Cu measured by EDS.

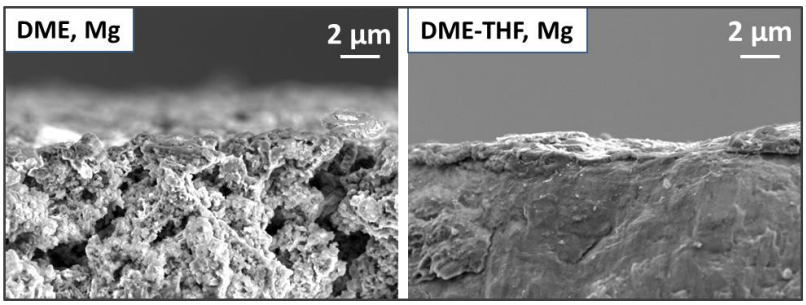

Fig. S11. SEM image of cross sections of the Mg anode cycled with DME (left) and DME-THF (right) electrolytes.

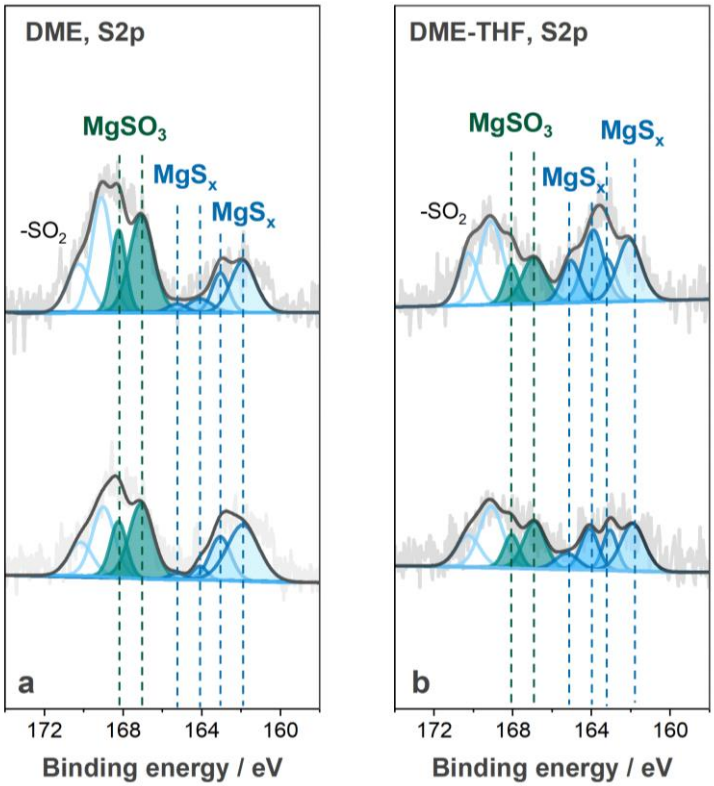

Fig. S12. S2p spectra of the Mg electrode cycled in (a) DME and (b) DME-THF electrolyte.

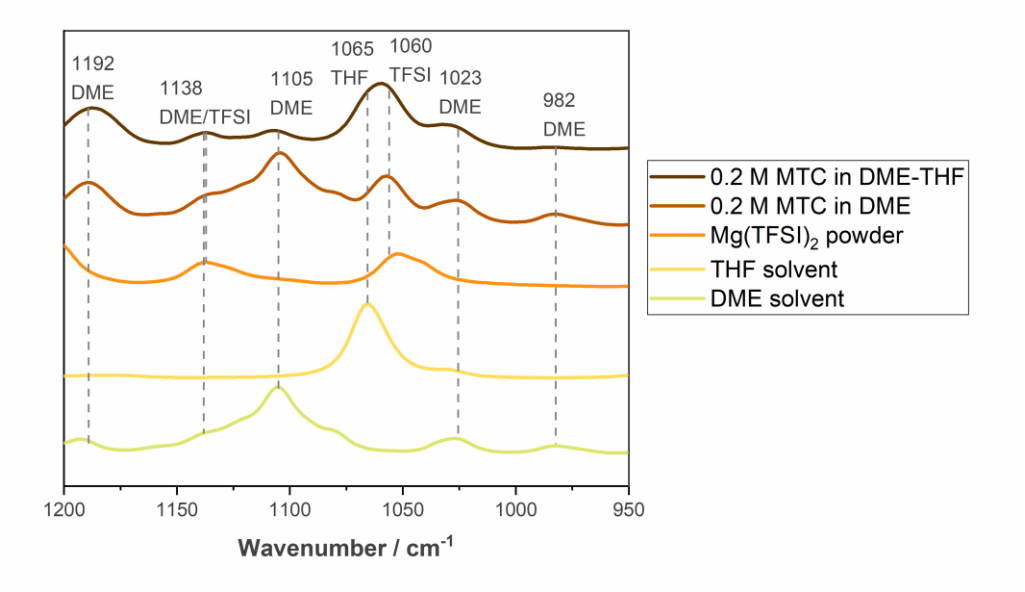

Fig. S13. FT-IR spectra of 0.2 M MTC in DME-THF, 0.2 M MTC in DME, $Mg(TFSI)_2$ powder, THF solvent, and DME solvent.

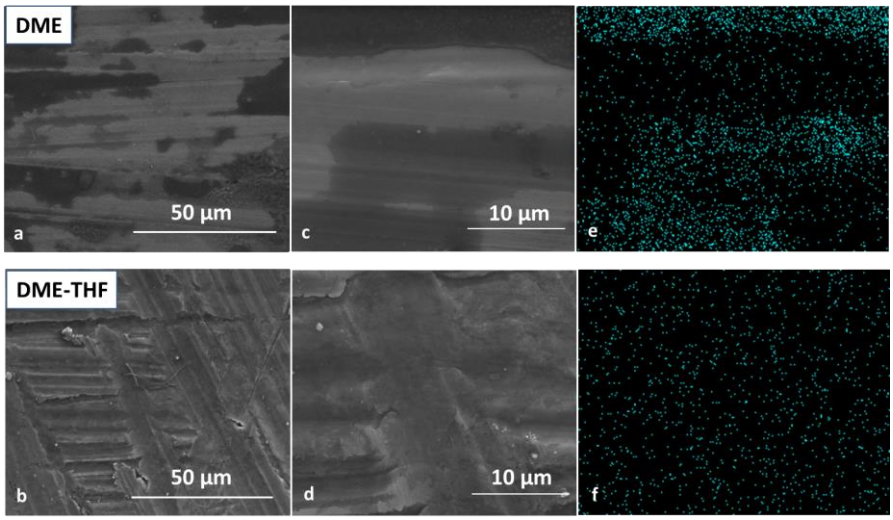

Fig. S14. The morphology of surface film on Mg anode soaked in (a), (c) DME and (b), (d) DME-THF electrolytes for 11 days. F element mapping of Mg anode soaked in (e) DME and (f) DME-THF electrolytes measured by EDS.

DFT calculations

In order to evaluate the optimal adsorption geometry, three adsorption sites (**Fig. S15a**, top, bridge and hollow of Mg) on Mg (1000) and four adsorption sites (**Fig. S15b**, top, bridge, hollow of Mg, and top of O) on MgO (100) surfaces were considered. The adsorption configurations were shown in **Fig. S15c-d.**

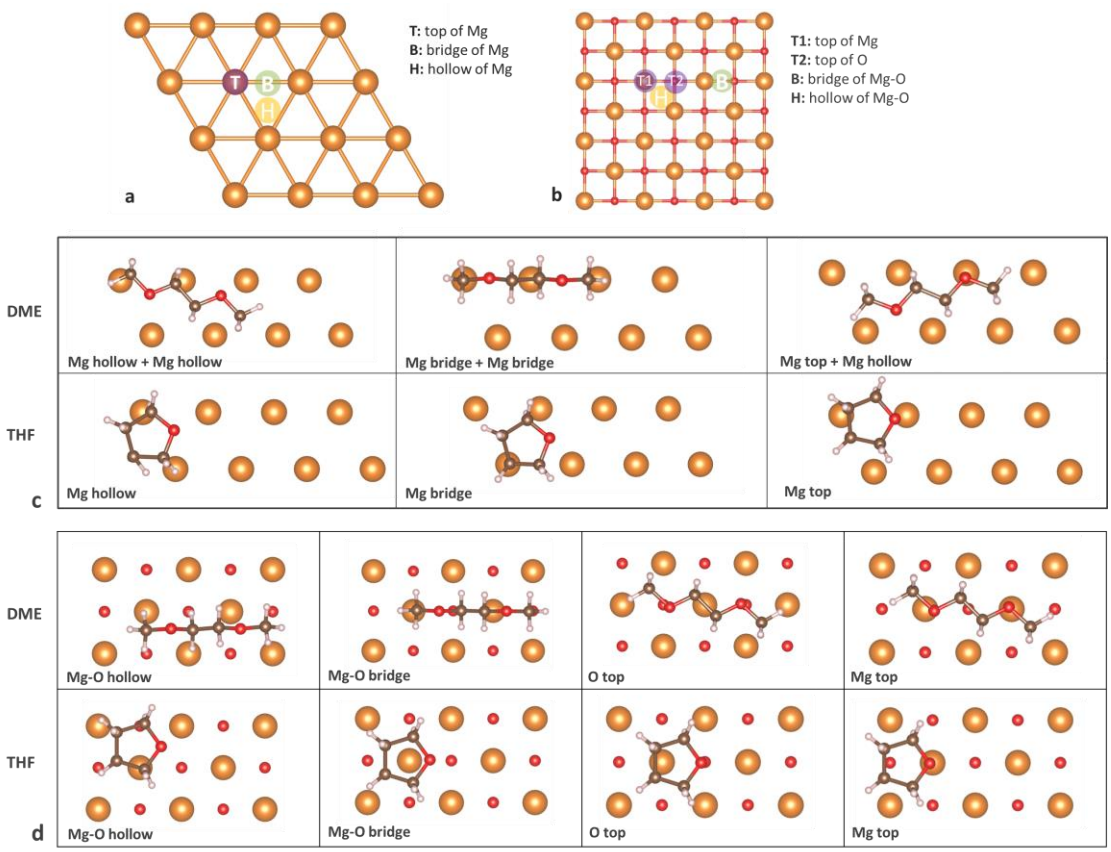

Fig. S15. (a) Top view of Mg (0001) surface and possible adsorption sites; (b) Top view of MgO (100) surface and possible adsorption sites. (c) Initial configurations of DME and THF on Mg (0001). (d) Initial configurations of DME and THF on MgO (100).

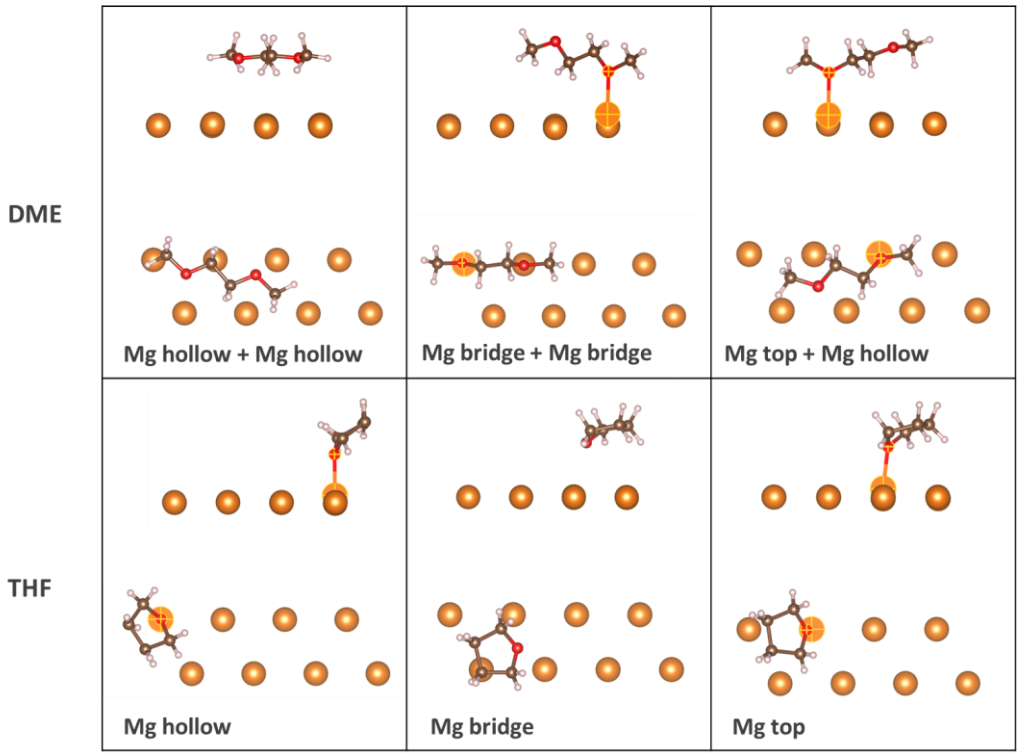

Fig. S16. Optimal configurations of DME and THF on Mg (0001).

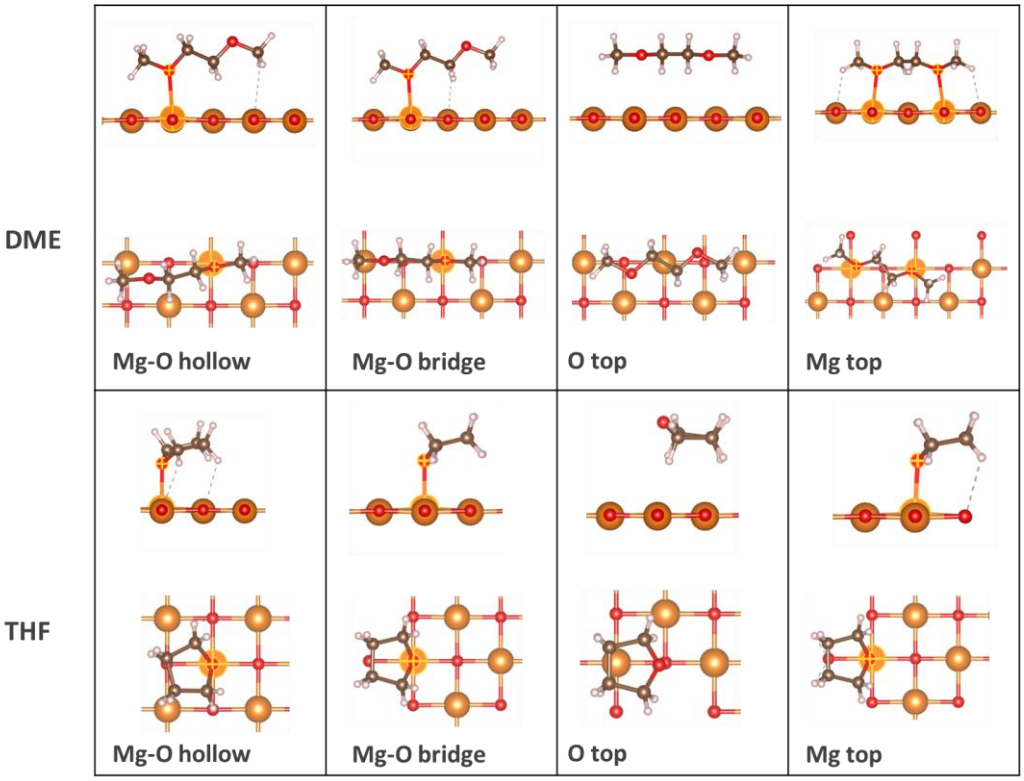

Fig. S17. Optimal configurations of DME and THF on MgO (100).

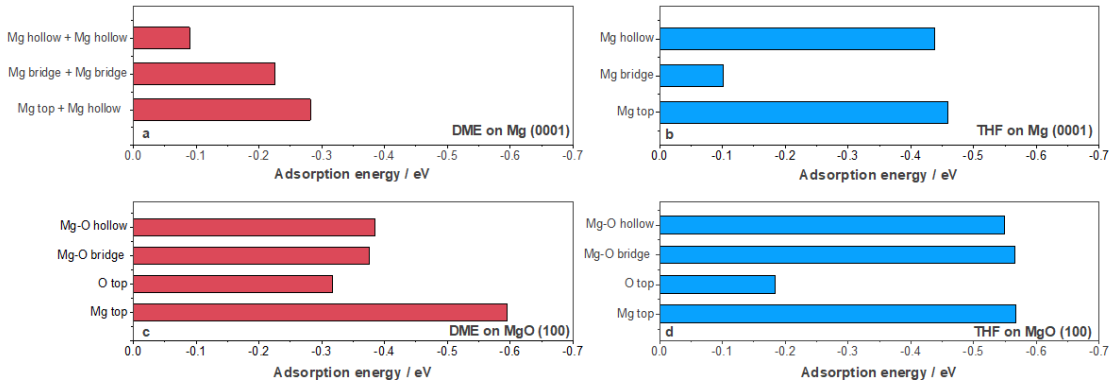

Fig. S18. Adsorption energy of (a) DME on Mg (0001) surface; (b) THF on Mg (0001) surface. (c) DME on MgO (100) surface. (d) THF on MgO (100) surface.

References

1 M. Mao, Z. Lin, Y. Tong, J. Yue, C. Zhao, J. Lu, Q. Zhang, L. Gu, L. Suo, Y.-S. Hu, H. Li, X. Huang and L. Chen, *ACS Nano*, 2020, **14**, 1102–1110.

2 B. D. Adams, J. Zheng, X. Ren, W. Xu and J.-G. Zhang, *Adv. Energy Mater.*, 2018, **8**, 1702097.

3 G. Kresse and J. Furthmüller, *Physical review B*, 1996, **54**, 11169.

4 G. Kresse and J. Furthmüller, *Computational materials science*, 1996, **6**, 15–50.

5 G. Kresse and D. Joubert, *Physical review b*, 1999, **59**, 1758.

6 J. P. Perdew, K. Burke and M. Ernzerhof, *Phys. Rev. Lett.*, 1996, **77**, 3865–3868.

7 P. E. Blöchl, *Phys. Rev. B*, 1994, **50**, 17953–17979.

8 S. Grimme, *J. Comput. Chem.*, 2006, **27**, 1787–1799.

9 J.-J. Tang, X.-B. Yang, L. OuYang, M. Zhu and Y.-J. Zhao, *J. Phys. D: Appl. Phys.*, 2014, **47**, 115305.

10 C. G. Johansen, H. Huang and T.-M. Lu, *Computational Materials Science*, 2009, **47**, 121–127.

11 J. G. Smith, J. Naruse, H. Hiramatsu and D. J. Siegel, *Chem. Mater.*, 2016, **28**, 1390–1401.

12 N.I.o. Standards, Technology, *NIST*.

13 K. Momma and F. Izumi, *Journal of Applied Crystallography*, 2011, **44**, 1272–1276.

14 C. Liebenow, Z. Yang and P. Lobitz, *Electrochemistry Communications*, 2000, **2**, 641–645.

15 D. Aurbach, Z. Lu, A. Schechter, Y. Gofer, H. Gizbar, R. Turgeman, Y. Cohen, M. Moshkovich and E. Levi, *Nature*, 2000, **407**, 724.

16 O. Mizrahi, N. Amir, E. Pollak, O. Chusid, V. Marks, H. Gottlieb, L. Larush, E. Zinigrad and D. Aurbach, *J. Electrochem. Soc.*, 2008, **155**, A103.

17 D.-T. Nguyen, A. Y. S. Eng, M.-F. Ng, V. Kumar, Z. Sofer, A. D. Handoko, G. S. Subramanian and Z. W. Seh, *Cell Reports Physical Science*, 2020, **1**, 100265.

18 N. Sa, B. Pan, A. Saha-Shah, A. A. Hubaud, J. T. Vaughey, L. A. Baker, C. Liao and A. K. Burrell, *ACS Appl. Mater. Interfaces*, 2016, **8**, 16002–16008.

19 S. He, K. V. Nielson, J. Luo and T. L. Liu, *Energy Storage Materials*, 2017, **8**, 184–188.

20 I. Shterenberg, M. Salama, H. D. Yoo, Y. Gofer, J.-B. Park, Y.-K. Sun and D. Aurbach, *J. Electrochem. Soc.*, 2015, **162**, A7118–A7128.

21 L. Yang, C. Yang, Y. Chen, Z. Pu, Z. Zhang, Y. Jie, X. Zheng, Y. Xiao, S. Jiao, Q. Li and D. Xu, *ACS Appl. Mater. Interfaces*, 2021, **13**, 30712–30721.

22 Y. He, Q. Li, L. Yang, C. Yang and D. Xu, *Angew. Chem. Int. Ed.*, 2019, **58**, 7615–7619.

23 K. A. See, K. W. Chapman, L. Zhu, K. M. Wiaderek, O. J. Borkiewicz, C. J. Barile, P. J. Chupas and A. A. Gewirth, *J. Am. Chem. Soc.*, 2016, **138**, 328–337.

24 Z. Zhao-Karger, M. E. Gil Bardaji, O. Fuhr and M. Fichtner, *J. Mater. Chem. A*, 2017, **5**, 10815–10820.

25 T. Mandai, *ACS Appl. Mater. Interfaces*, 2020, **12**, 39135–39144.

26 O. Tutusaus, R. Mohtadi, T. S. Arthur, F. Mizuno, E. G. Nelson and Y. V. Sevryugina, *Angewandte Chemie International Edition*, 2015, **54**, 7900–7904.

27 H. Dong, O. Tutusaus, Y. Liang, Y. Zhang, Z. Lebens-Higgins, W. Yang, R. Mohtadi and Y. Yao, *Nat Energy*, 2020, **5**, 1043–1050.

28 J. Xiao, X. Zhang, H. Fan, Y. Zhao, Y. Su, H. Liu, X. Li, Y. Su, H. Yuan, T. Pan, Q. Lin, L. Pan and Y. Zhang, *Advanced Materials*, 2022, 2203783.

29 K. Tang, A. Du, S. Dong, Z. Cui, X. Liu, C. Lu, J. Zhao, X. Zhou and G. Cui, *Adv. Mater.*, 2020, **32**, 1904987.

30 K. Tang, A. Du, X. Du, S. Dong, C. Lu, Z. Cui, L. Li, G. Ding, F. Chen, X. Zhou and G. Cui, *Small*, 2020, **16**, 2005424.

31 S. Hou, X. Ji, K. Gaskell, P. Wang, L. Wang, J. Xu, R. Sun, O. Borodin and C. Wang, *Science*, 2021, **374**, 172–178.

32 Y. Han, G. Li, Z. Hu, F. Wang, J. Chu, L. Huang, T. Shi, H. Zhan and Z. Song, *Energy Storage Materials*, 2022, **46**, 300–312.

33 H. Fan, Z. Zheng, L. Zhao, W. Li, J. Wang, M. Dai, Y. Zhao, J. Xiao, G. Wang, X. Ding, H. Xiao, J. Li, Y. Wu and Y. Zhang, *Adv. Funct. Mater.*, 2020, **30**, 1909370.

34 S.-Y. Ha, Y.-W. Lee, S. W. Woo, B. Koo, J.-S. Kim, J. Cho, K. T. Lee and N.-S. Choi, *ACS Appl. Mater. Interfaces*, 2014, **6**, 4063–4073.

35 C. Liao, N. Sa, B. Key, A. K. Burrell, L. Cheng, L. A. Curtiss, J. T. Vaughey, J.-J. Woo, L. Hu and B. Pan, *Journal of Materials Chemistry A*, 2015, **3**, 6082–6087.